Fertilization-driven Pulses of Atmospheric Nitrogen Dioxide Complicate Air Pollution in Early Spring over the North China Plain

Tian Feng,[1] Guohui Li,[2,*] Shuyu Zhao,[3] Naifang Bei,[4] Xin Long,[5] Yuepeng Pan,[6] Yu Song,[7] Ruonan Wang,[2] Xuexi Tie,[2] Luisa T. Molina[8]

[1] Department of Geography & Spatial Information Techniques, Ningbo University, Ningbo, China
[2] KLACP, State Key Laboratory of Loess and Quaternary Geology, Institute of Earth Environment, Chinese Academy of Sciences, Xi'an, China
[3] Ningbo Meteorological Bureau, Ningbo, China
[4] School of Human Settlements and Civil Engineering, Xi'an Jiaotong University, Xi'an, China
[5] Research Center for Atmospheric Environment, Chongqing Institute of Green and Intelligent Technology, Chinese Academy of Sciences, Chongqing, China
[6] State Key Laboratory of Atmospheric Boundary Layer Physics and Atmospheric Chemistry (LAPC), Institute of Atmospheric Physics, Chinese Academy of Sciences, Beijing, China
[7] State Key Joint Laboratory of Environmental Simulation and Pollution Control, Department of Environmental Science, Peking University, Beijing, China
[8] Molina Center for Energy and the Environment, La Jolla, CA, USA

*Corresponding author. Email: ligh@ieecas.cn

Abstract

Atmospheric nitrogen dioxide (NO_2) has shown periodic conspicuous pulses in tropospheric column in March over the North China Plain during the past two decades. However, these repetitive pulses have never been reported and its underlying causes remain unclear. Here, we present robust evidence to demonstrate that agricultural fertilization drives the early-spring NO_2 column increases. The fertilization-driven soil NO_x (=NO+NO_2) emissions, comparable to anthropogenic sources, exert complicated influences on regional air quality. They significantly reduce nocturnal and diurnal O_3 concentrations in agricultural areas in early spring, distinct from the scenarios in summer, but increase fine particulate matter ($PM_{2.5}$) concentrations via strongly enhancing nitrate aerosol formation. The impact also extends to urban areas, approximately half that of agricultural areas. These findings are with increasing implications for coordinated control of $PM_{2.5}$ and O_3 under global warming. We thus suggest that reducing NO_x emissions in croplands is essential to achieve better air quality in agricultural countries and regions.

Short Summary

Impacts of agricultural fertilization on nitrogen oxide and air quality are becoming more pronounced with continuous reductions in fossil fuel sources in China. We report that atmospheric nitrogen dioxide pulses driven by agricultural fertilizations largely complicate air pollution in the North China Plain, highlighting the necessity of agricultural emission control.

Keywords: Nitrogen Dioxide, Fertilization, Air Pollution, Ozone, $PM_{2.5}$

1 Introduction

Nitrogen oxide (NO_x = nitric oxide (NO) + nitrogen dioxide (NO_2)) is a major air pollutant in the troposphere and a key precursor to ozone (O_3) and fine particulate matter ($PM_{2.5}$) due to its photochemical properties (Seinfeld and Pandis, 2006; Zhang et al., 2015). It is also a short-lived climate forcer regulated by both China and the United States (IPCC, 2023). Understanding the NO_x budget is crucial for addressing these issues. Globally, atmospheric NO_x is mainly produced by fossil fuel combustion (Crippa et al., 2023; Janssens-Maenhout et al., 2015; Yan et al., 2005), with smaller contributions from wildfires and lightning (Bauwens et al., 2020; Murray et al., 2012). Additionally, soil generates substantial NO_x through nitrification and denitrification processes (Bouwman et al., 2002; Cárdenas et al., 1993; Davidson, 1992; Yan et al., 2005), particularly after the rewetting of dry soils (Galbally and Roy, 1978; Huber et al., 2020; Yienger and Levy, 1995). On a regional scale, soil NO_x emissions maybe even exceed those from fossil fuel sources in summer (Almaraz et al., 2018; Sha et al., 2021). Model- and satellite-based studies estimate that global annual soil NO emissions, with the largest contributor of cultivated croplands, range from 9 to 27 Tg N (Hudman et al., 2012; Steinkamp and Lawrence, 2011; Vinken et al., 2014; Yan et al., 2005), accounting for about 15% of total NO_x emissions (Hudman et al., 2012). This wide range is due to the complex response of soil NO_x emissions to driving factors like fertilization, temperature, and soil moisture (Huber et al., 2020; Oikawa et al., 2015), making accurate estimation challenging.

The emission rates from fertilized croplands are 1 to 2 orders of magnitude higher than nearby grasslands and forest soils (Almaraz et al., 2018; Anderson and Levine, 1987; Guo et al., 2020; Yienger and Levy, 1995). Recent studies show significant NO_x emissions from croplands post-fertilization, exceeding pre-fertilization rates by an order of magnitude (Almaraz et al., 2018; Hickman et al., 2017; Laville et al., 2011; Liu et al., 2005; Oikawa et al.,

2015; Zhao et al., 2015). Despite these robust evidences of strong NO_x emissions from agricultural fertilization, the lack of extensive *in-situ* measurements hinders accurate estimation of these emissions and their environmental impacts. Additionally, the effect of agricultural fertilization on air quality has not received sufficient global attention, although some pioneering studies have pointed the implications for air quality since the 1990s (Davidson et al., 1998; Hall et al., 1996). In recent years, studies have reported that agricultural soil emissions significantly increase atmospheric NO_x levels (Almaraz et al., 2018; Hickman et al., 2017; Huang et al., 2018; Oikawa et al., 2015) and enhance O_3 formation in summer in California (Oikawa et al., 2015) or during the growing season of crops in sub-Saharan Africa (Hickman et al., 2017; Huang et al., 2018).

The North China Plain (NCP) is one of the major grain-producing regions in China. Winter wheat-maize double cropping is a typical rotation system mainly practiced in this region (Liu et al., 2003; Zhu et al., 1994). China has been the world's largest consumer of N-fertilizer since 2000 (Liu et al., 2013), with annual usage peaking at approximately 31.2 Tg N in 2014 (Yu et al., 2022). About half of this fertilizer is lost to the environment (Liu et al., 2013), indicating a significant potential source for NO_x emissions from China's croplands. The agricultural management in the NCP has been known for incorporating high fertilization rates according to the solar terms with excessive N fertilization (Sun et al., 2022; Vitousek et al., 2009; Zhao et al., 2006). Thus, this region is primarily responsible for agricultural N-fertilizer consumption (Yu et al., 2022) and has shown substantial soil NO_x emissions (Liu et al., 2010; Tang et al., 2020; Zhang et al., 2011). The emissions significantly increase ambient NO_x levels and enhance O_3 formation in summer (Huang et al., 2023; Lu et al., 2021; Wang et al., 2022). These concerns typically focus on the warm season when higher temperatures favor NO_x emissions from soils. However, frequent agricultural activities and N-fertilizer use also occur during

transitional seasons, and how periodic agricultural fertilization affects soil NO_x emission and regional air quality remains unclear.

In this study, we present an unexpected pulse of atmospheric NO_2 column in early spring during the past two decades over the NCP. However, this phenomenon has not been previously reported in this region. Combining agricultural fertilization records, surface NO_2 and NH_3 observations, long-term satellite observations of NO_2 and NH_3, and a flexible scheme of soil NO_x emission, we explain successfully the underlying cause for the NO_2 column peaks using a regional atmospheric transport model online coupled with chemistry, and further assess the impacts of the pulsing NO_x emission on reginal air quality.

2 Materials and Methods

2.1 Model and configurations

The Weather Research and Forecasting model fully coupled with atmospheric chemistry (WRF-Chem, version 3.6.1) we used is a modified model by Li et al. (2011a; 2012; 2010; 2011b) and Feng et al (2021), in which we implement the BDSNP mechanism by Hudman et al. (2012) to calculate soil NO_x emission related to agricultural fertilization and the influences on regional air quality in the NCP. The model is configured with grid spacing of 6 km × 6 km (240 × 280 grid cells) with the center at 38°N and 116°E (Figure 1). Thirty-five vertical levels are employed in the stretched vertical grid with spacing ranging from 50 m near surface, to 500 m at 2.5 km and 1 km above 14 km. Meteorological initial and boundary conditions use the National Centers for Environmental Prediction (NCEP) FNL 1°×1° analysis data, and the chemical initial and boundary conditions are interpolated from the CAM-Chem 6-h output (Buchholz et al., 2019; Emmons et al., 2020). The non-soil emission inventory is developed by Zhang et al. (2009) and the biogenic emissions are calculated online using the Model of Emissions of Gases and Aerosol from Nature (MEGAN) model (Guenther et al., 2006).

Specifically, monthly ammonia (NH_3) emissions are incorporated from a high-resolution NH_3 emission inventory developed by Huang et al., (2012), which includes emissions from fertilizer application, livestock, and other sources. The model spin-up time is 2 days (Table 1).

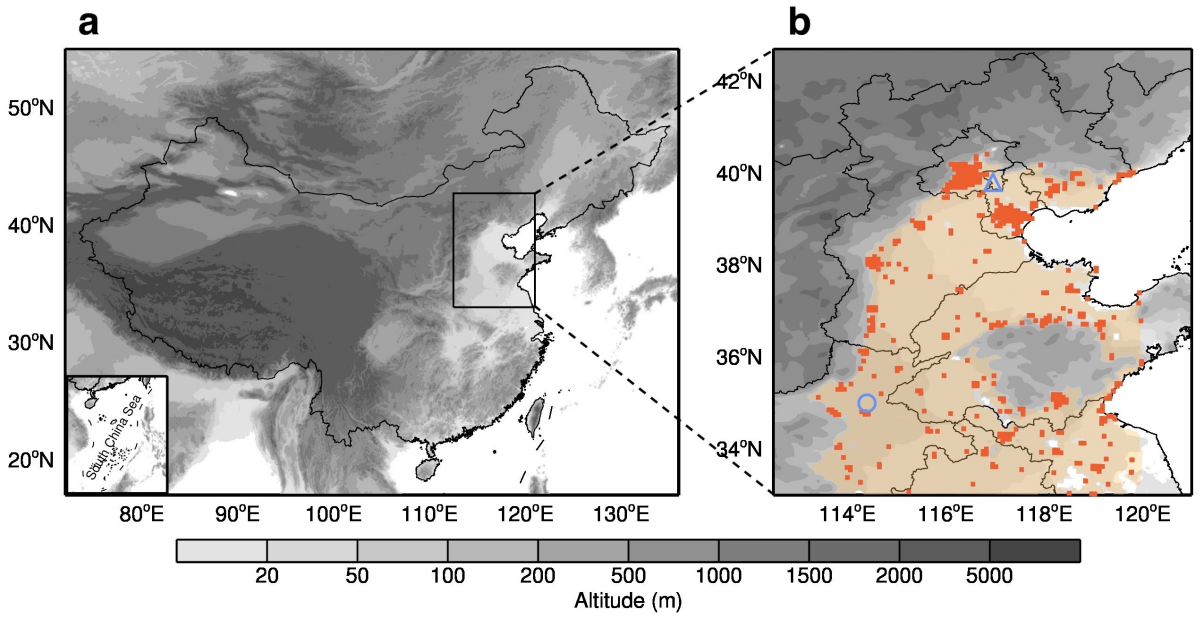

Figure 1. Domain overview. (a) Geographic location of the NCP, which is predominantly characterized by plains at an elevation less than 100 m, and known for a major agricultural zone. (b) Extensive cultivated croplands distribute in the NCP, marked by the orange shadings, while urban areas are marked by red shadings. The graphic markers denote locations of field observation sites, of which the blue circle represents the Fengqiu cropland ecological station, Chinese Academy of Sciences, with a long-term record on agricultural fertilization, and the triangle represents the rural Xianghe station with ambient NH_3 measurements. The agricultural areas in orange within the NCP are defined as croplands with altitude less than 100 m, and the urban areas in red are defined as built-up areas within the NCP.

Table 1. Model configuration for the simulation domain, meteorological schemes, initial and boundary conditions, and emission inventories.

Item	Configuration
Period	February through April, 2020
Region	The NCP and surrounding areas
Domain center	116°E, 38°N
Domain size	1440 km × 1680 km
Horizontal resolution	6 km × 6 km
Vertical resolution	35 vertical levels with a stretched vertical grid with spacing ranging from 50 m near surface, to 500 m at 2.5 km and 1 km above 14 km
Microphysics scheme	WRF Single-Moment 6-class scheme (Hong and Lim, 2006)
Boundary layer scheme	MYJ TKE scheme (Janjić, 2002)
Surface layer scheme	MYJ surface scheme (Janjić, 2002)
Land-surface scheme	Noah land surface model (Chen and Dudhia, 2001)
Longwave radiation scheme	New Goddard scheme (Chou et al., 2001)
Shortwave radiation scheme	New Goddard scheme (Chou and Suarez, 1999)
Meteorological boundary and initial condition	NCEP FNL 1° × 1° analysis data
Chemical boundary and initial condition	CAM-Chem 6-h output (Buchholz et al., 2019; Emmons et al., 2020)
Anthropogenic emission inventory	MEIC emission inventory (Li et al., 2017c; Zhang et al., 2009), except for NH_3
NH_3 emission inventory	NH_3 emission inventory in China (Huang et al., 2012)
Biogenic emission inventory	MEGAN model (2006)
NO_x emission from various types of soils	Soil NO_x emission mechanism (2012)
Spin-up time	2 days

2.2 Soil NO_X emission scheme

We implement a soil NO_x emission scheme, the Berkeley-Dalhousie Soil NO Parameterization (BDSNP) by Hudman et al. (2012), into the WRF-Chem model. The scheme comprehensively considers various factors, including available soil nitrogen content (N_{avail}, ng N m^{-2}) from the fertilizer application and nitrogen deposition, in which the soil NO_x emission (E_{soil}, ng N m^{-2} s^{-1}) is a function of N_{avail}, climate, and edaphic conditions:

$$E_{soil} = A'_{biome}(N_{avail}) \times f(T) \times g(\theta) \times P(l_{dry}) \quad (1)$$

where N_{avail} is available soil nitrogen mass, and A'_{biome} (ng N m^{-2} s^{-1}) represents the biome-dependent emission factor. $f(T)$ (dimensionless) and $g(\theta)$ (dimensionless) are parameters

regulated by soil temperature and moisture, respectively. $P(l_{dry})$ (dimensionless) denotes the pulsed soil emission from wetting of dry soils. The product by $f(T)$ and $g(\theta)$ is calculated following:

$$f(T) \times g(\theta) = e^{0.103T} \times a\theta e^{-b\theta^2} \quad (2)$$

where T ($0 \leq T \leq 30°C$) is soil temperature and θ ($0 \leq \theta \leq 1$, dimensionless) is water-filled pore space, defined as the ratio of the volumetric soil moisture content to the porosity. According to the laboratory and field measurements (Hudman et al., 2012), the constants a and b are determined so that $g(\theta)$ maximizes when $\theta = 0.2$ for arid soils and $\theta = 0.3$ elsewhere.

The pulsing term $P(l_{dry})$, following Yan et al. (2005), describes the magnitude of the peak flux relative to the pre-wetting flux, which is parameterized as:

$$P(l_{dry}) = [13.01 \ln(l_{dry}) - 53.6] \times e^{-ct} \quad (3)$$

where l_{dry} (hours) represents the length of the antecedent dry period, and c (c = 0.068 h^{-1}) is a constant rate denoting the rise/fall time of the pulse. Fertilizer applications data are interpolated from the global gridded chemical fertilizer and manure application inventory at 0.5°× 0.5° (Potter et al., 2010; Yan et al., 2005). The chemical and manure fertilizers are obtained from the International Fertilizer Association (IFA) and the Food and Agriculture Organization of the United Nations (FAO). The Chinese chemical fertilizer application (straight N application) from IFA is about 19.6 Tg N a^{-1} for 2000, quite close to the amount of 19.9 Tg N a^{-1} for 2020 from the China Statistical Yearbook (https://www.stats.gov.cn/sj/ndsj/2021/indexch.htm). More details of the scheme are found in related studies elsewhere (Hudman et al., 2012; Lu et al., 2021).

2.3 Emission inventories

We employ two emission inventories in this study, of which the Hemispheric Transport of Air Pollution Version 3 (HTAP v3, 2005-2018) emission inventory includes soil and non-soil

emissions (Li et al., 2017b), and the Multi-resolution Emission Inventory for China (MEIC v1.3, 2007-2018) has no soil emission (Li et al., 2017b). In the HTAP inventory, the non-soil emission inventory includes energy, industry, ground transport, residential, waste, shipping and aviation sources in the HTAP inventory, with a spatial resolution of 0.1°×0.1° and a temporal resolution of one month. Agricultural emissions are involved in the latest HTAP v3 inventory, which includes soil NO_x emissions (Crippa et al., 2023). Nevertheless, the soil emissions in this inventory are calculated using traditional "bottom-up" method (Kurokawa and Ohara, 2020), rather than estimated by a process-based emission module. The monthly MEIC emission inventory with a spatial resolution of 0.25°×0.25° is incorporated in parallel with the HTAP emission inventory. Here, we focus on NO_x and NH_3 emissions from croplands with fertilization, and adopt NH_3 emission inventory by Huang et al. (2012) because they explicitly distinguish NH_3 produced by agricultural fertilization from other NH_3 sources.

2.4 Air pollutant measurements

Satellite-derived tropospheric NO_2 columns are from OMI hosted by the Aura satellite that is launched by the National Aeronautics and Space Administration (NASA). The Level-3 product, where pixel level data of good quality are binned and "averaged" into 0.25°×0.25° grids, was retrieved and analyzed in the present study. The dataset is for all atmospheric conditions, and for sky conditions with cloud fraction less than 30% (https://cmr.earthdata.nasa.gov/search/concepts/C1266136111-GES_DISC.html). The Level-2 product of NH_3 columns is employed, which is from the Space Administration and the Infrared Atmospheric Sounding Interferometer (IASI) hosted on the MetOp series of satellites. Both of the satellites operate in a sun-synchronous polar orbit and have a local overpass time of around 13:45 (local time, LT) (once a day) and 9:30 am / 9:30 pm (twice a day), respectively, in North China. The tropospheric column of NO_2 screened for cloud fraction less than 30% global daily

composite, has a spatial resolution of 13 km × 24 km, with a temporal coverage of 2005-2022 (Lamsal et al., 2021), and the trajectory NH_3 from IASI is integrated into each 0.125° × 0.125° grid cell with the average during 2007-2021 (Clarisse et al., 2023). Low-quality satellite data are filtered out due to the interference of clouds. To cover all the domain (Figure 1), the data used in this study are merged into seven-day mean datasets of NO_2 and NH_3 columns with a non-overlapping 7-day window. The data are interpolated into the model grids using bilinear interpolation.

Ambient surface NO_2, O_3, and $PM_{2.5}$ mass concentrations at 141 sites in the NCP are from the China National Environmental Monitoring Centre (CNEMC, Figure S1). These *in-situ* measurements are performed by the Thermo Scientific™ ambient particulate monitor and gas analyzers, of which NO_2 and O_3 are measured by Model 42i Chemiluminescence NO-NO_2-NO_x Analyzer, Model 49i UV Photometric Ozone Analyzer, respectively. $PM_{2.5}$ is measured by Model 5030 Synchronized Hybrid Ambient, Real-time Particulate (SHARP) Monitor, which uses proprietary digital filtering to continuously calibrate mass to obtain an accurate, precise and real-time mass concentration. The sampling time is 1 min for these monitoring devices, which is averaged for hourly data. Agricultural NH_3 concentration is monitored by a Picarro analyzer based on the principle of cavity ring-down spectroscopy (CRDS) at the rural Xianghe station (Figure 1), with a sampling frequency of 1 Hz.

3 Results and Discussion

3.1 Satellite-retrieved NO_2 column pulses

During the past two decades, seven-day mean tropospheric column of NO_2 measured by the Ozone Monitoring Instrument (OMI) in the NCP exhibits a significant temporal variation, with the magnitude varying from less than 100 μmol m^{-2} to more than 680 μmol m^{-2} (Figure 2a). The annual cycle is highly prominent and its seasonal variation is remarkable, with

significantly higher levels in cold seasons than those in warm seasons. Throughout the year, the pattern of NO_2 column looks like a rhinoceros horn, which is characterized by a major peak in winter and multiple noticeable sub-peaks in other seasons. These sub-peaks often occur at fixed times, such as in March, June and October, of which the sub-peak is the most noticeable in March, with the highest magnitude (Figures 2a and S1). We examine the monthly variation in anthropogenic NO_x emission rates over the NCP in global and regional emission inventories, and find that the monthly variation is more evident in the regional emission inventory, with a significantly higher emission than that in the global emission inventory. Nevertheless, neither of them reveals any discernible sub-peaks of NO_x emission rates from fossil fuel combustion to coincide with the sub-peaks of the NO_2 column (Figure 2b).

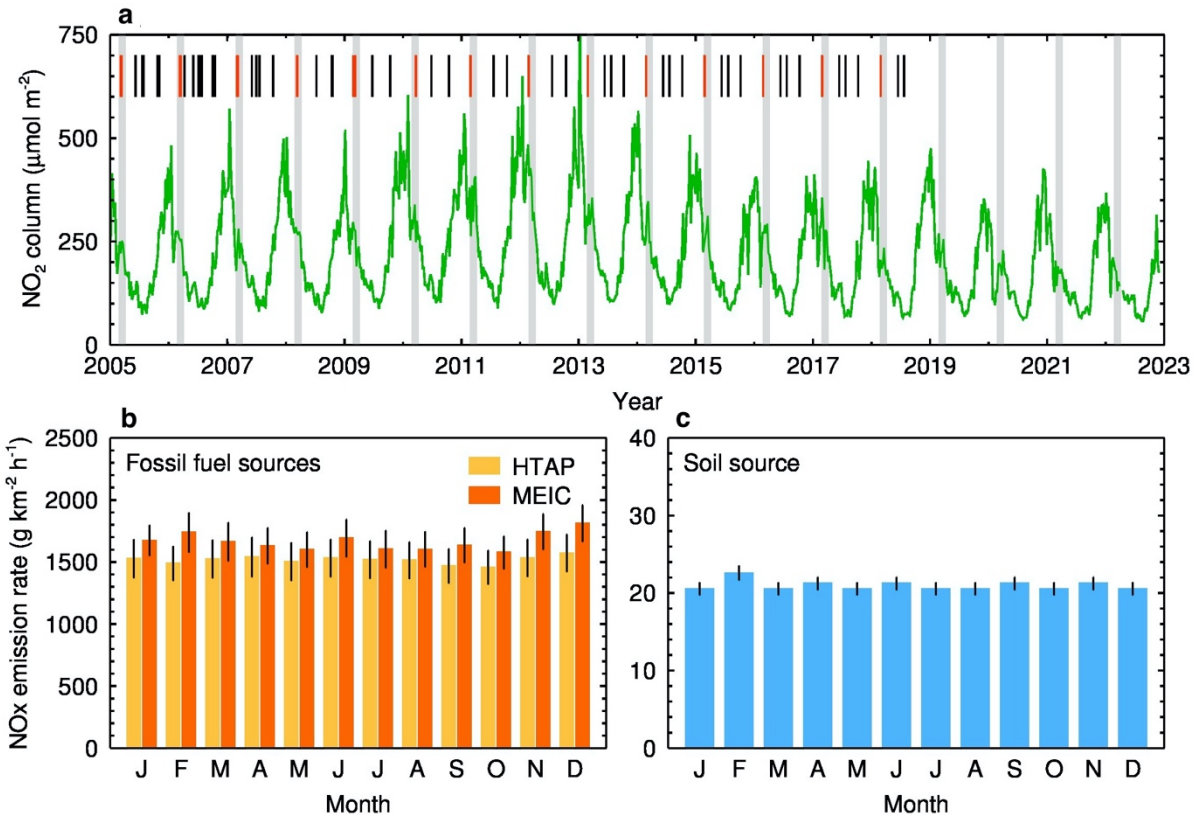

Figure 2. NO_2 column pulses in March and NO_x emissions from fossil fuel and soil sources over the NCP. (a) Long-term variation of seven-day mean tropospheric NO_2 column observed by OMI during the past two decades (2005-2022). Intersections of the gray bars and the green lines denote a sub-peak of NO_2 column occurred in each March, and the short bars represent

the timing record for agricultural fertilization at Fengqiu station in the NCP, of which the red ones indicate the fertilization period in early spring. (b) Monthly mean NO_x emission rates with ±1**σ** standard deviation (SD) in two sets of anthropogenic emission inventories, the HTAP v3 (2005-2018, orange) and MEIC v1.3 (2008-2017, red). (c) Same as (b), but for NO_X emission rates from soils in the HTAP v3 inventory (2005-2018).

As for soil NO_x emissions, they are absent in the regional emission inventory, while in the global emission inventory, soil NO_x emissions fluctuate slightly on a monthly scale, far less than those from fossil fuel combustion, constituting less than 2% of the total (Figure 2c). Similar to NO_x emissions from fossil fuel combustion, there are no evident sub-peaks of soil NO_x emission to keep pace with the atmospheric NO_2 column. Soil NO_x emissions are even at a lower level in March, significantly less than emissions in adjacent months. Therefore, the known emission inventory fails to explain the occurrence of these sub-peaks. On the other hand, we compute a pollution accumulation index (PAI, Text S1), the product of boundary layer height and wind speed, to semi-quantitatively assess the influence of atmospheric dispersion conditions on NO_2 column. NO_2 column seems to be somewhat dependent on the PAI, yet the noticeable discrepancies between the timing of the sub-peaks and PAI are insufficient to account for the occurrence of each sub-peak (Figure S3). Additionally, it is seen that the daily soil temperature was consistently higher than 0°C during March 2020 and the ten days before. Therefore, the sub-peak of NO_2 column is not expected to be originated from soil thaw either.

3.2 Linkage between NO_2 column pulses and agricultural fertilization

What causes these regular NO_2 sub-peaks occurred over the NCP during the past two decades? Measurements on ammonia (NH_3) column also present similar pulses to those of NO_2 column during the same period, in spite of some differences in the long-term trend (Figures S3 and S4).

These concurrent sub-peaks of NH_3 column provide favorable evidence that these NO_2 column sub-peaks are likely connected to agricultural activities because atmospheric NH_3 is largely originated from fertilizer application in agriculture (Crippa et al., 2023; Huang et al., 2012; Li et al., 2017b). Another key evidence is that the occurrence of each sub-peak of the NO_2 column is highly consistent with the record of agricultural fertilization at the Fengqiu cropland ecological station in the NCP during the past decades (Figures 1b, 2a, and S1). The wheat-maize double-cropping system is predominate in the NCP, where the agricultural activities are strongly dependent on the lunar calendar. For winter wheat, the planting date ranges from early to mid-October (after maize harvest). Fertilization is generally divided into three stages: 1) Pre-planting during late September – early October; 2) Jointing stage during mid-March – early April; 3) Grain filling during late April for high-yield fields. The planting date of summer maize ranges from early to mid-June (after wheat harvest), and the stages of fertilization include: 1) At planting during early June; 2) V6-V8 stage during early July; 3) Tasseling stage during late July for high-yield fields. The agricultural fertilization is closely associated with three solar terms, i.e., Waking of Insects in March (the 3rd solar term), Grain in Beard in June (the 9th solar term) and Cold Dew in October (the 17th solar term). As already mentioned, two different satellite products reveal significant and concurrent pulses of NO_2 column and NH_3 column around these three solar terms (Figures 2a, S1, S3, and S4), indicating that they are likely originated from the same sources. During these pulses of the NO_2 column, we found that the pulse in March is more pronounced than those in June and October, because March is the season for a large-scale cultivating in the NCP, accompanied by more land preparation and fertilization. Therefore, we hypothesize that the NO_2 column pulse in March is possibly caused by fertilized croplands that accelerate NO_x emissions from agricultural soils. Field campaigns have measured a high NO emission rate of 266.3 g km^{-2} h^{-1} in croplands after fertilization and irrigation in autumn in eastern China (Tang et al., 2020; Tian et al., 2020) and also other regions

(Hickman et al., 2017; Huang et al., 2018; Huber et al., 2020), suggesting that agricultural fertilization is likely a significant source of atmospheric NO_x in major agricultural countries like China.

3.3 Soil NO_x emission mechanism

To examine the role of soil NO_x emissions from agricultural fertilization in the pulses of atmospheric NO_2 column, we introduce a flexible soil NO_x emission module and NH_3 emission into the WRF-Chem model, and perform two simulation experiments that include and exclude soil emissions, respectively (Table 1). Noticeably, there is an acceleration in the release of soil NO_x, and daily mean emission rate increases from 155.6 g km^{-2} h^{-1} to 438.3 g km^{-2} h^{-1} during the simulation period (Figure 3a). In particular, the NO_x emission rate during the post-fertilization phase is significantly higher than those during other phases, consistent with the accelerated soil NO_x release observed in agricultural areas in California after fertilization (Oikawa et al., 2015). On average, the simulated NO_x emission rate in March is 312.9 g km^{-2} h^{-1}, between the measured 113.6 g km^{-2} h^{-1} in November in eastern China (Tang et al., 2020) and 988.2 g km^{-2} h^{-1} in September in California (Oikawa et al., 2015), suggesting the rationality of the soil NO_x emission mechanism in the model.

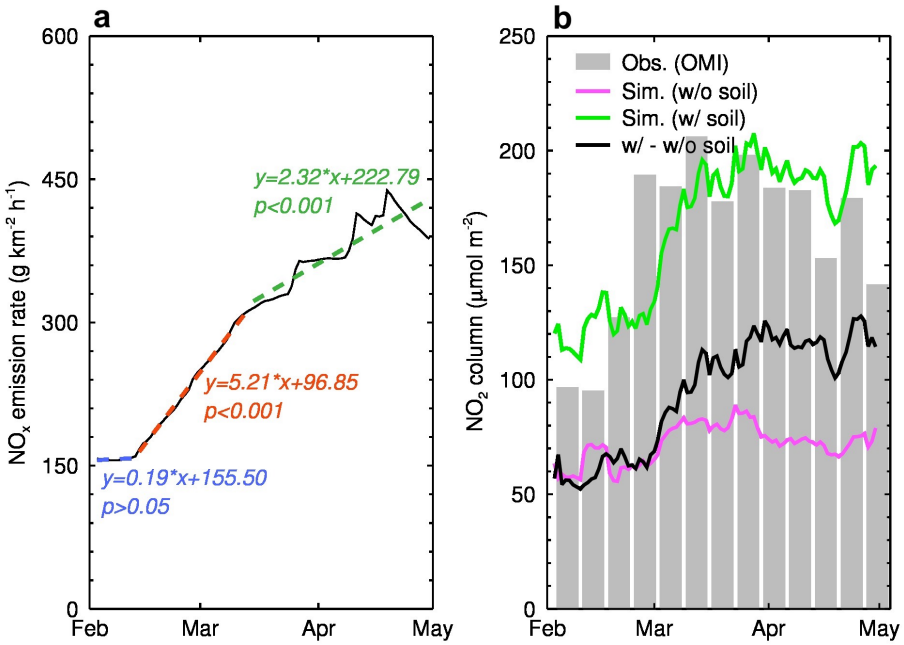

Figure 3. NO_x emissions from agricultural fertilization and resultant NO_2 column during February-April in 2020 over the NCP. (a) Calculated NO_x emission rate from croplands with N-fertilizer application in the model. The black curve represents daily variation in NO_x emission rate around the fertilization, and the blue, red, and green dash lines correspond to the trends of NO_x emission rates in croplands during the pre-fertilization, fertilization and post-fertilization periods, respectively. (b) Observed and simulated NO_2 column. The gray histogram represents NO_2 column observed by satellite (OMI). The green and pink lines represent simulated NO_2 column with and without soil NO_x emissions, and the black line shows the difference between them. The model well replicates the rapid increase in observed NO_2 column by considering soil NO_x emissions from agricultural fertilization.

We evaluate the model performance against satellite-derived NO_2 column. Consequently, the modified model perfectly replicates the sudden increase in NO_2 column linked to agricultural fertilization, while the conventional WRF-Chem model fails to capture the observed NO_2 column pulse in March due to lack of the adopted soil NO_x emission mechanism (Figure 3b). For example, when soil NO_x emission caused by agricultural fertilization is

considered, the simulated NO_2 column rapidly increases to the peak in March, matching well with the satellite observation. However, without the contribution of agricultural fertilization, NO_2 column seems to exhibit a weak upward trend, but not significant. Comparing these two scenarios, a substantial NO_x emission from N-fertilizer input in croplands leads to an increase in NO_2 column by 1 to 1.5 times.

We also validate the modified model performance on temporal variations of routine surface pollutant measurements (NO_2, O_3 and $PM_{2.5}$) associated with NO_x emissions at the CNEMC sites throughout the simulation period (Figure 4). Although there are some discrepancies between the simulations and observations, e.g., overestimates occur in mid-February for NO_2 and $PM_{2.5}$ levels, the model generally reproduces hourly variations in each pollutant reasonably. The IOAs between the simulated and observed near-surface concentrations of NO_2, O_3, and $PM_{2.5}$ are 0.90, 0.91, and 0.88, respectively, and the normalized mean biases (NMBs) for these pollutants are within 10%.

We still cannot ignore the discrepancies between the model results and observations. These biases may largely originate from the soil NO_x emission mechanism. The fertilization dates in the BDSNP mechanism are determined by the beginning and end of the growing season that is derived from the MODIS Land Cover Dynamics product (MCD12Q2) averaged over the years from 2001 to 2004 (Hudman et al., 2012). This may be quite different from practices in 2020, the year we simulated in this study. We use the default assumption in the mechanism that 75% of fertilizer is added at the green-up day with the remaining 25% applied constantly throughout the rest of the season (Hudman et al., 2012). Though the 75/25 treatment is the most typical global farming practice (Matson et al., 1998), it may probably introduce extra biases in a specific region. Despite the uncertainties, all of these significant improvements of the modified model we used suggest that soil NO_x emission from agricultural fertilization would exert a crucial influence on regional air quality.

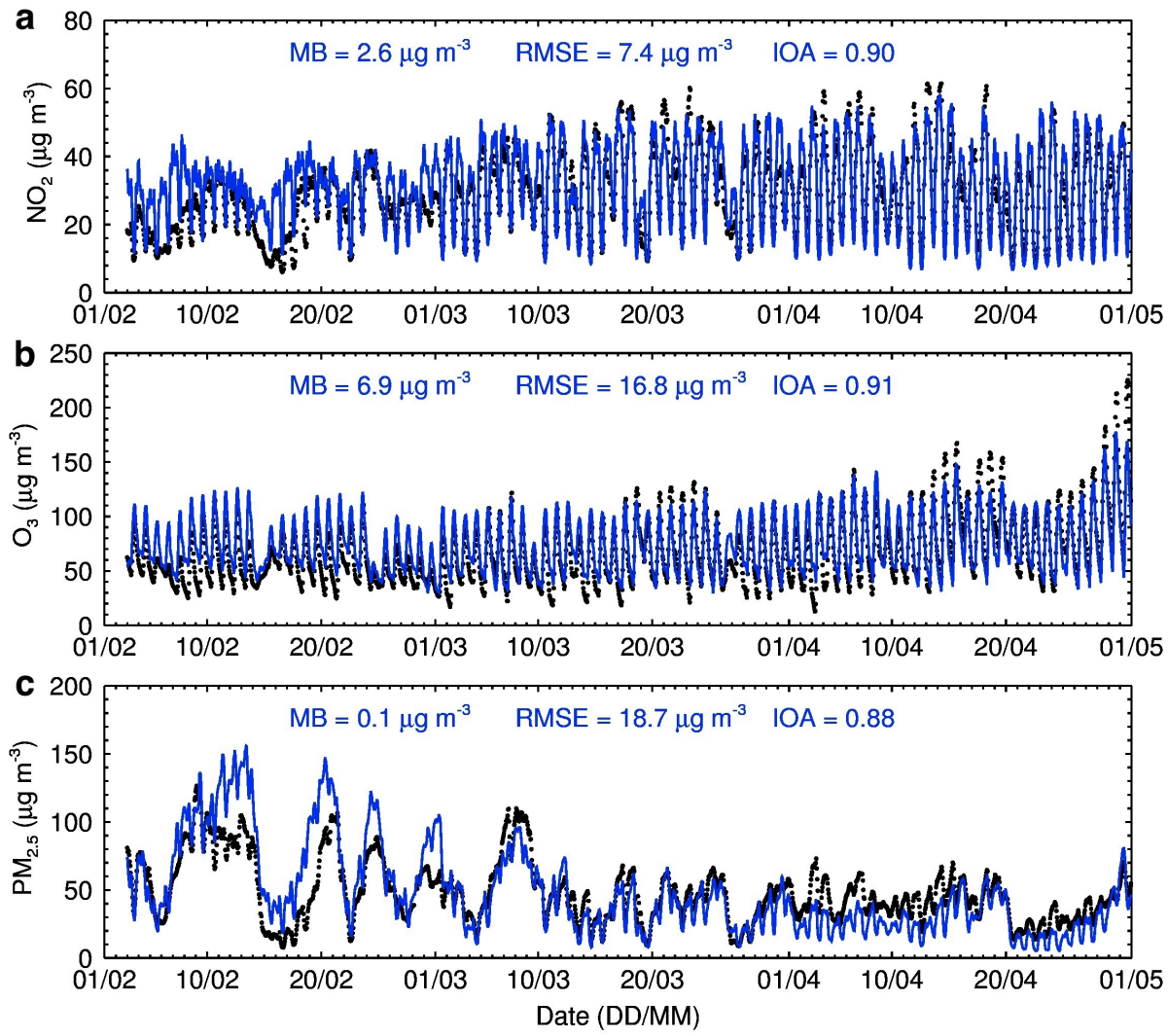

Figure 4. Simulated *vs.* measured surface pollutants averaged over the monitoring sites of the NCP (Figure S1) during February-April in 2020. (a to c) Temporal variations in surface NO_2 (a), O_3 (b), and $PM_{2.5}$ (c) mass concentrations. The blue curves denote the model calculation and the black dots denote *in-situ* measurements. Model biases are shown in the central upper position of each figure.

Furthermore, we examine the ability of the model to simulate the ground-level NO_2 mass concentration and NH_3 volume concentration when soil NO_x rapidly releases after fertilization. The reason is that influences of soil emissions on atmospheric NO_2 and NH_3 concentrations are confined in the near-surface layers below 1 km, and the influences diminish rapidly as

altitude increases (Figure 5). This indicates that impact of the soil emissions is primarily concentrated near the ground surface. With soil emissions included or not in the model, we compare the simulated NO_2 and NH_3 concentrations with near-surface observations (Figures 6a and 6b). When there are no soil NO_x emissions from agricultural fertilization, the simulated NO_2 concentration is significantly lower than the observed by 10.8 μg m^{-3}. While considering these emissions, the mean bias (MB, Text S2) between the simulation and the observation decreases to 2.1 μg m^{-3}, and the index of agreement (IOA, Text S2) also increases from 0.49 to 0.86. Similarly, the simulated NH_3 concentration is in good agreement with the observed when the soil NH_3 emission related to agricultural fertilization is involved, e.g., the MB decreases from 11.5 ppb to 2.0 ppb, and the IOA increases from 0.55 to 0.76 (Figures 6c and 6d). It is important to acknowledge the limitation posed by the absence of direct comparisons with flux measurements of NO_x emissions from soils, due to the unavailability of such data. The simulated NO_x emission flux from the BDSNP scheme cannot be well examined, which may introduce uncertainties to the predicted emission rates and mixing ratios in the atmosphere.

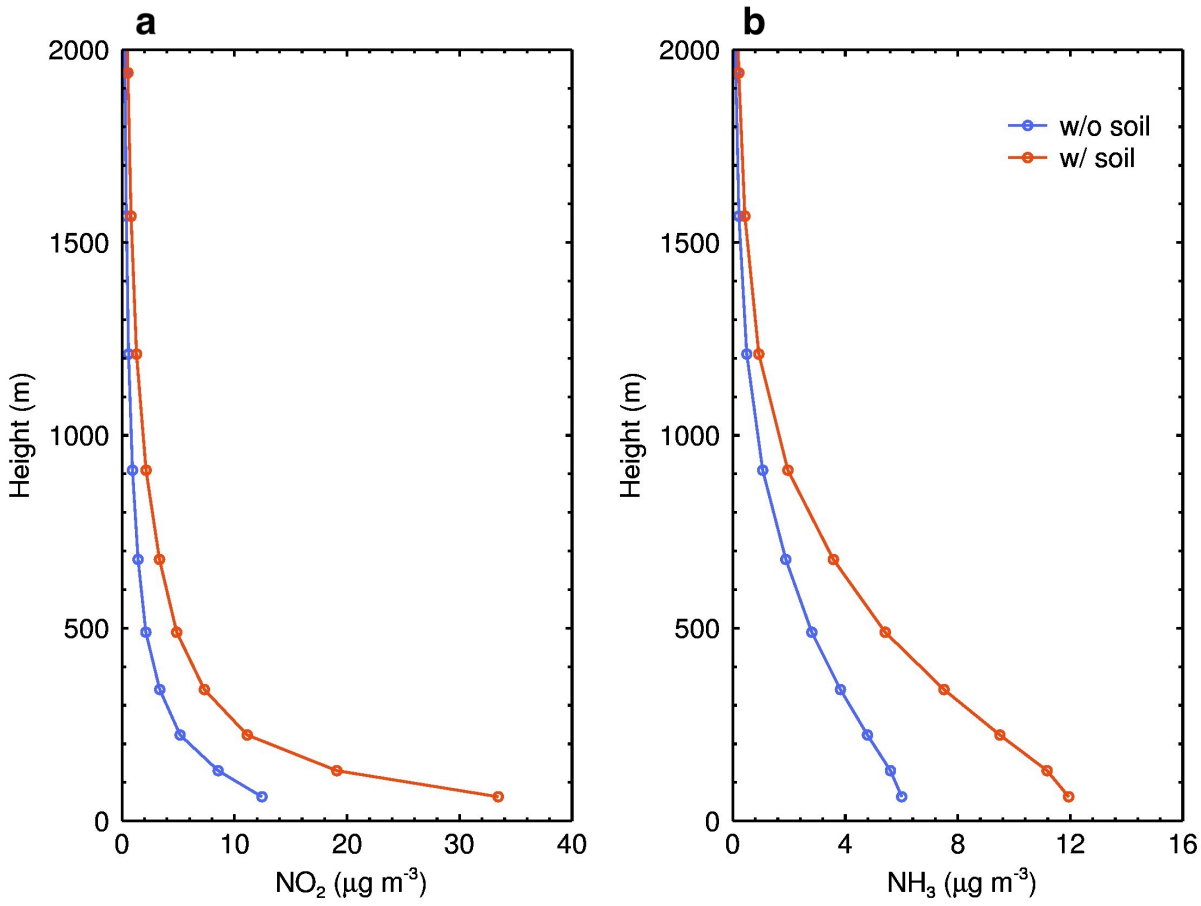

369

370 Figure 5. Vertical profiles for impacts of soil emissions on gas pollutants during March 2020

371 over the NCP. (a) Difference in NO_2 concentration with and without the influence of soil NO_x

372 emission from agricultural fertilization at various heights in the near-surface layers. (b) Similar

373 to (a), but for NH_3 concentration.

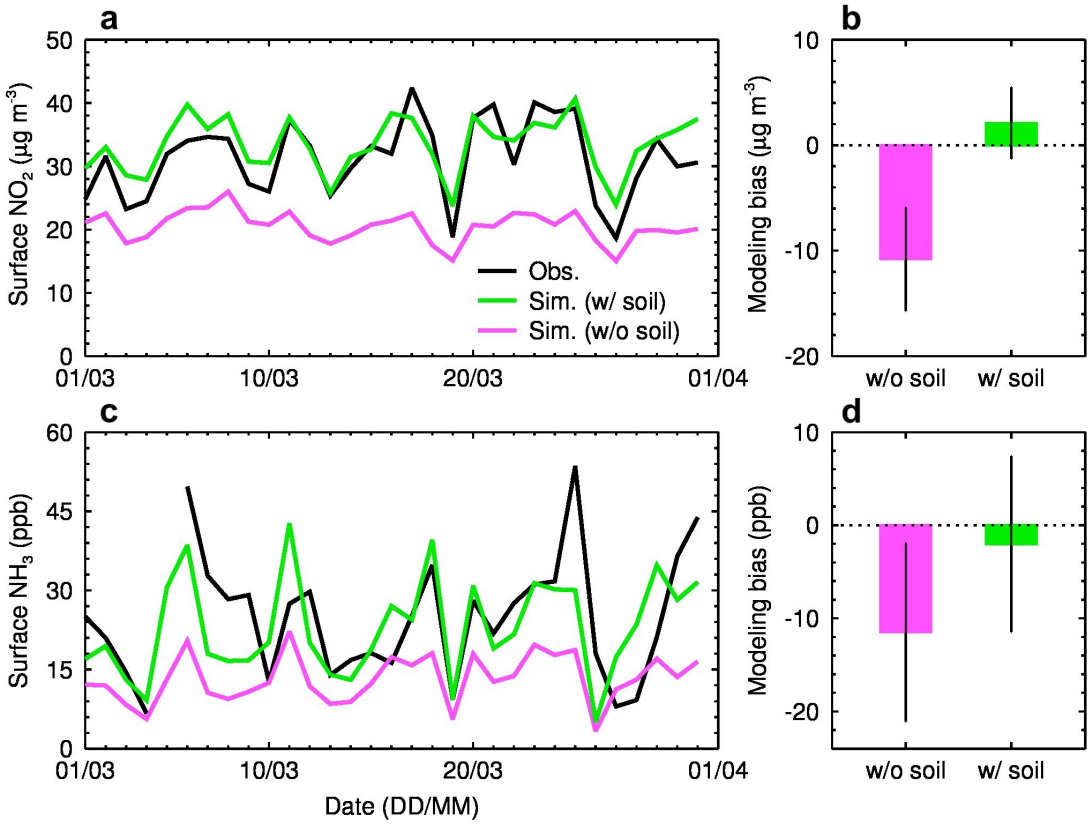

Figure 6. Contribution of soil emissions from agricultural fertilization on surface NO_2 and NH_3 during March 2020 over the NCP. (a-b) Change in surface NO_2 concentration with (green) and without (pink) soil NO_X emission from agricultural fertilization, the black line in (a) is for observed surface NO_2 concentration. (c-d) Same as (a-b), but for NH_3. The error bar in (b and d) denotes ±1**σ**. NO_2 observations are averaged over the 141 monitoring stations in the study area from the CNEMC network. NH_3 observations are from the rural Xianghe station (Figure 1). According to *in-situ* measurements on NO_2 and NH_3, the units for NO_2 and NH_3 concentrations are μg m^{-3} and ppb, respectively.

3.4 Significance of soil NO_x emissions from agricultural fertilization for air quality

We perform a model experiment that excludes the soil sources in the study domain to examine the impacts of soil emissions on regional air quality. The model results are compared to the benchmark scenario with soil sources involved to examine these impacts. Agricultural fertilization directly leads to substantial increases in atmospheric NO_x and NH_3 concentrations.

According to the spatial correlation between land use and NO_2 concentration, NO_2 concentrations increase by more than 15 μg m^{-3} over agricultural areas, with the maximal increments occurring in the densely cultivated southern region of the NCP, exceeding 40 μg m^{-3} (Figures 1b and 7a). While in urban areas, the increase in NO_2 concentration is mostly below 10 μg m^{-3}, significantly lower than those in agricultural areas. This indicates that the influence of local emissions originated from agricultural fertilization on air quality primarily concentrate in agricultural areas. Nonetheless, the influence extends to surrounding areas through atmospheric transport, leading to an inhomogeneous increase of NO_2 concentrations across the NCP. Spatial distribution of the increased NH_3 concentration is highly similar to that of the increased NO_2 concentration, but some differences exist in the southeast of the NCP. It should be noted that the NH_3 emission in the model is from Huang et al. (2012), a separate monthly emission inventory. The emission rates of NH_3 in the southeast of the NCP is lower than that of NO from the BDSNP scheme. This indicates nonnegligible discrepancies in the derived emissions between these two approaches, which deserves more in-depth studies.

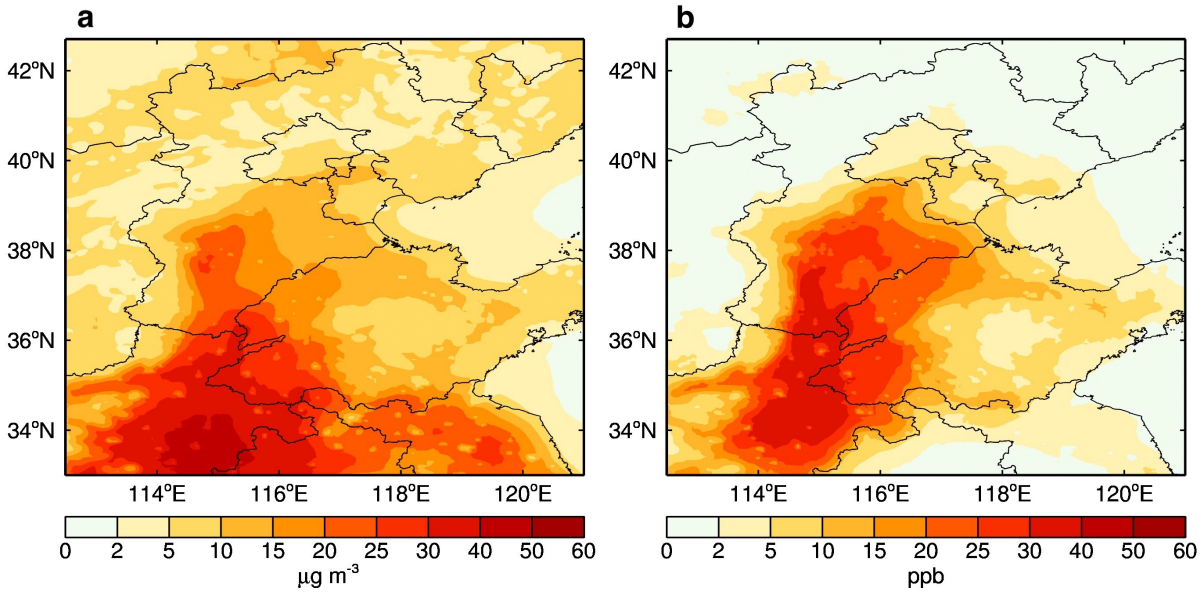

Figure 7. Direct impacts of soil emissions from agricultural fertilization on surface NO_2 and NH_3 during March 2020 over the NCP. (a and b) Spatial distributions of changes in surface NO_2 and NH_3 concentrations due to fertilization-related soil emissions. According to *in-situ*

407 measurements on NO_2 and NH_3, the units for NO_2 and NH_3 concentrations are μg m^{-3} and ppb,
408 respectively.
409
410 A substantial amount of reactive nitrogen from agricultural fertilization suddenly enters
411 the atmosphere, and further affects air quality via photochemical reactions and aerosol
412 chemical transformations profoundly (Seinfeld and Pandis, 2006; Wu et al., 2020). Our results
413 reveal that the NO_x emission induced by N-fertilization significantly suppresses the early-
414 spring O_3 production in the NCP, which varies remarkably with the land use, approximately
415 twice as strong in agricultural areas as in urban areas. For instance, in agricultural areas, the
416 emission in croplands reduces nocturnal and diurnal O_3 by 30.1±6.5 μg m^{-3} (37.5±8.1%) and
417 15.0±3.7 μg m^{-3} (18.7±4.6%), respectively, while in urban areas, the corresponding O_3
418 reductions are 15.6±4.7 μg m^{-3} (15.6±4.7%) and 9.7 ±3.2 μg m^{-3} (10.6±3.4%), respectively
419 (Figure 8). Based on the diurnal cycle of the change in O_3 concentrations ($\Delta[O_3]$), we also find
420 that the nighttime O_3 reduction is much higher than the daytime reduction (Figure 9). The $\Delta[O_3]$
421 caused by agricultural fertilization is linearly and negatively correlated with the change in NO_2
422 concentration ($\Delta[NO_2]$) (Figures 10a-d), and the negative correlation is more pronounced at
423 night ($r < -0.99$ and $p < 0.001$ for both the agricultural and the urban areas, Figures 10a and b).
424 This suggests that the O_3 concentration strongly depends on the change in NO_x levels in the
425 NCP during early spring. Continuous agricultural NO_x (mainly NO) emissions inhibit the O_3
426 formation by NO titration when the solar radiation is weak (Feng et al., 2021; Li et al., 2017a),
427 particularly at night without sunlight. On the other hand, a negative correlation between $\Delta[NO_2]$
428 and the change in daytime OH radical ($\Delta[OH]_{day}$) suggests that the $\Delta[NO_2]$ also moderately
429 regulates $\Delta[OH]_{day}$ ($r = -0.50$ for agricultural areas and $r = -0.43$ for urban areas, $p < 0.001$,
430 Figures 10e and f) through decreasing O_3 levels and reactions of NO_2 with OH radical. Both
431 OH radical and O_3 are critical oxidants in the atmosphere, and the decrease by the excessive

NO_x emission from agricultural fertilization weakens atmospheric oxidizing capacity (AOC) (Feng et al., 2021). The decreased AOC can further slow down the oxidation processes in homogeneous and heterogeneous reactions, unfavorable for the formation of secondary aerosols. We note that soil nitrous acid (HONO) emission can also perturb atmospheric chemistry and the AOC (Feng et al., 2022; Tan et al., 2023) via providing NO and OH through photolysis. The emission rate of HONO from soil is much less than that of NO_x in the NCP (Tan et al., 2023), which increases daytime O_3 and OH concentrations slightly during summer (Feng et al., 2022; Tan et al., 2023). However, the influence in springtime still remains to be elucidated.

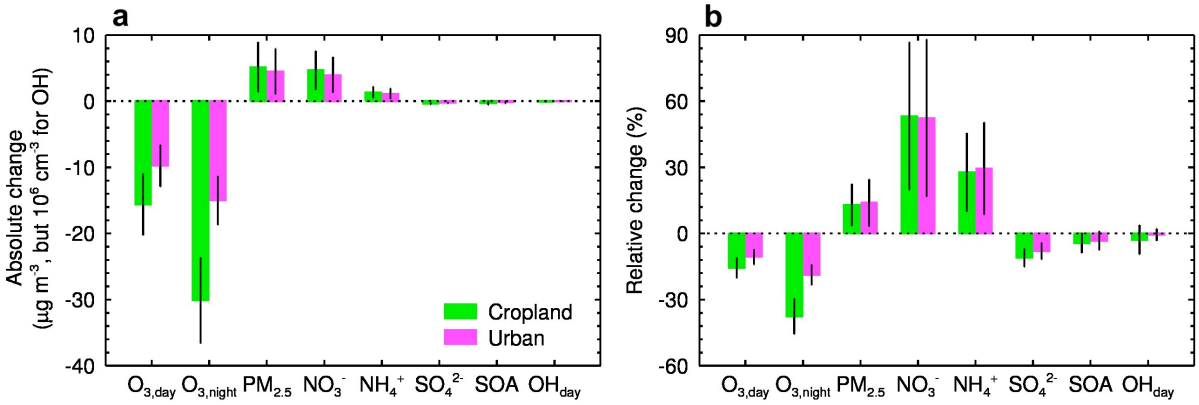

Figure 8. Complex impacts of agricultural fertilization on O_3, $PM_{2.5}$, and OH during March 2020 over the NCP. (a) Changes in mass concentrations of O_3, $PM_{2.5}$, aerosol constituents, i.e., nitrate, ammonium, sulfate and secondary organics, and OH radical due to soil NO_x emission from agricultural fertilization in agricultural (green) and urban (pink) areas. The error bar denotes $\pm 1\boldsymbol{\sigma}$. (b) Same as (a), but for percentage changes.

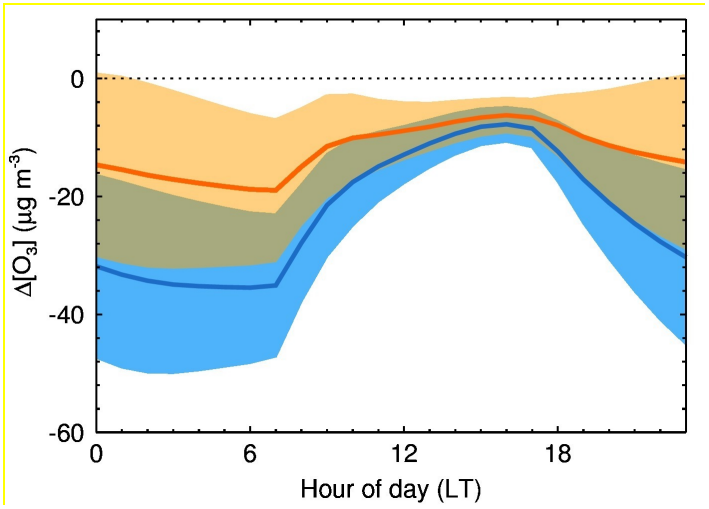

447

448 Figure 9. Secondary impact of soil NO_x emissions from agricultural fertilization on surface O_3
449 during March 2020 over the NCP. Diurnal cycles of changes in surface O_3 concentrations due
450 to fertilization-related soil emissions over croplands and urban areas in the NCP. The blue and
451 orange shadings show ±1**σ** of the data.

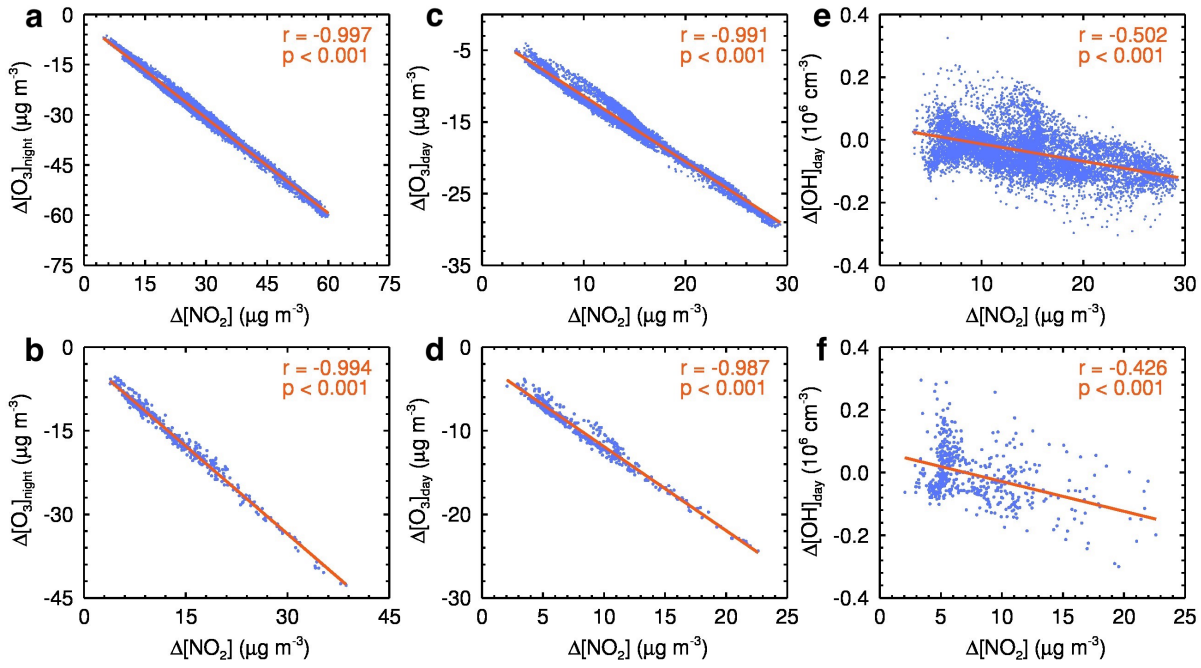

452

453 Figure 10. Changes in surface NO_2 and related photochemical products. (a to f) Correlation
454 between Δ[NO_2] and Δ[O_3] or Δ[OH] during March 2020 over the NCP. (a to d) Change in O_3
455 concentration is strongly dependent on change in NO_2 concentration due to agricultural
456 fertilization in both agricultural (a and c) and urban (b and d) areas, and the dependence is more

457 pronounced at night, i.e., correlation coefficient r = -0.997 (r = -0.994) at night and r = -0.991
458 (r = -0.987) at daytime in agricultural (urban) areas. (e and f) Change in daytime OH radical is
459 also significantly influenced by change in NO_2 concentration in both agricultural (e) and urban
460 (f) areas.
461
462 Interestingly, these findings regarding the impacts of soil NO_x emission on O_3 formation
463 in spring are different from previous studies revealing that agricultural NO_x emissions enhance
464 the O_3 formation in summer over the NCP (Huang et al., 2023; Lu et al., 2021; Tan et al., 2023;
465 Wang et al., 2022) and northeast China (Shen et al., 2023) and in the Imperial Valley, California
466 (Oikawa et al., 2015). Similar scenarios are also reported during the growing season of crops
467 in sub-Saharan Africa (Hickman et al., 2017; Huang et al., 2018). This is largely attributed to
468 the sensitivity of O_3 to its precursors under different conditions of solar radiation. During early
469 spring, the insolation is relatively weak, unfavorable for the O_3 photochemical production in
470 the NCP. As a result, a large amount of agricultural NO_x (mainly NO) emission even causes a
471 NO titration effect during daytime, decreasing O_3 concentrations, when the O_3 chemistry is
472 under the VOC-sensitive or the transitional regimes (Figure S6) (Sillman, 1995). In contrast,
473 the intensified solar radiation in summer significantly facilitates the O_3 photochemical
474 production, shifting the O_3 chemistry from VOCs-sensitive to NO_x-sensitive (Sha et al., 2021;
475 Wang et al., 2022). In this scenario, the O_3 production is primarily controlled by NO_x emissions,
476 meaning that the O_3 concentration increases with rising NO_x levels. This seasonal difference
477 in O_3 sensitivity to its precursors highlights a seasonally dependent response of O_3 production
478 to agricultural fertilization.
479 We also quantify the impact of agricultural fertilization on $PM_{2.5}$ concentrations. The NCP
480 is characterized by an excess of NH_3, in which nitrate formation is highly sensitive to NO_2
481 concentration and AOC due to NO_2 oxidation to NO_3^- via gas-phase and heterogeneous

482 reactions (Feng et al., 2018; Fu et al., 2020; Liu et al., 2019; Wen et al., 2018). As atmospheric
483 NO_2 and NH_3 concentrations rapidly increase due to emissions from fertilized croplands,
484 nitrate aerosol in agricultural (urban) areas rises by 4.7 (4.0) μg m^{-3}, corresponding to the
485 increased percentage of 53.2% (52.3%), while ammonium aerosol rises by 1.3 (1.1) μg m^{-3} in
486 agricultural (urban) areas, with an increased percentage of 27.7% (29.4%) (Figure 8). However,
487 sulfate aerosol shows a slight decrease both in agricultural and urban areas (Figure 8a). The
488 reason is that an extra NO_x emission from agricultural fertilization enhances nitrate formation
489 but lowers AOC, which hinders sulfate formation. Similar to sulfate aerosol, secondary organic
490 aerosol (SOA) also has a slight reduction (Figure 8a). The formation of SOA greatly depends
491 on the AOC level, so decreased AOC due to NO_x emission from agricultural fertilization does
492 not favor the conversion of organic precursors, such as VOCs and semi-volatile primary
493 organic aerosols, into SOA.

494 In general, due to the NO_x emission from agricultural fertilization, $PM_{2.5}$ concentration
495 increases by 5.1 (4.5) μg m^{-3} (Figure 8a), corresponding to a percentage change of 12.9%
496 (13.9%) over agricultural (urban) areas in the NCP (Figure 8b). There is no significant
497 difference in $PM_{2.5}$ increments between agricultural and urban areas. Nitrate aerosol is
498 primarily responsible for the increased $PM_{2.5}$, accounting for 92.2% and 88.9% in these two
499 types of regions, respectively. Our results also indicate that changes in $PM_{2.5}$ and nitrate in
500 urban areas are more sensitive to the change in NO_2 concentration. For instance, the ratios of
501 nitrate change to NO_2 change ($\Delta[NO_3^-]/\Delta[NO_2]$ = 0.20) and $PM_{2.5}$ change to NO_2 change
502 ($\Delta[PM_{2.5}]/\Delta[NO_2]$ = 0.24) in urban areas are both higher than those in agricultural areas
503 ($\Delta[NO_3^-]/\Delta[NO_2]$ = 0.13 and $\Delta[PM_{2.5}]/\Delta[NO_2]$ = 0.15, Figures 11a and b), indicating that the
504 conversion of NO_2 to nitrate aerosol is more efficient in urban areas. Consequently, the
505 increased percentages of $PM_{2.5}$ and ammonium aerosol in urban areas are higher than those in
506 agricultural areas (Figure 8b). Additionally, the ongoing stringent control measures on emission

sources significantly reduce anthropogenic emissions in urban areas, thus the impact of agricultural fertilization on urban air quality is becoming more pronounced (Figure S7). Since soil NO_x emission is sensitive to soil temperature, as global warming is ongoing, routine events like agricultural fertilization will continue to have amplified impacts on air quality with the joint help of atmospheric dispersion/transport and chemical transformation processes (Bennetzen et al., 2016; Ma et al., 2022; Tubiello et al., 2013). These impacts are not confined in agricultural areas alone, but extend to surrounding cities.

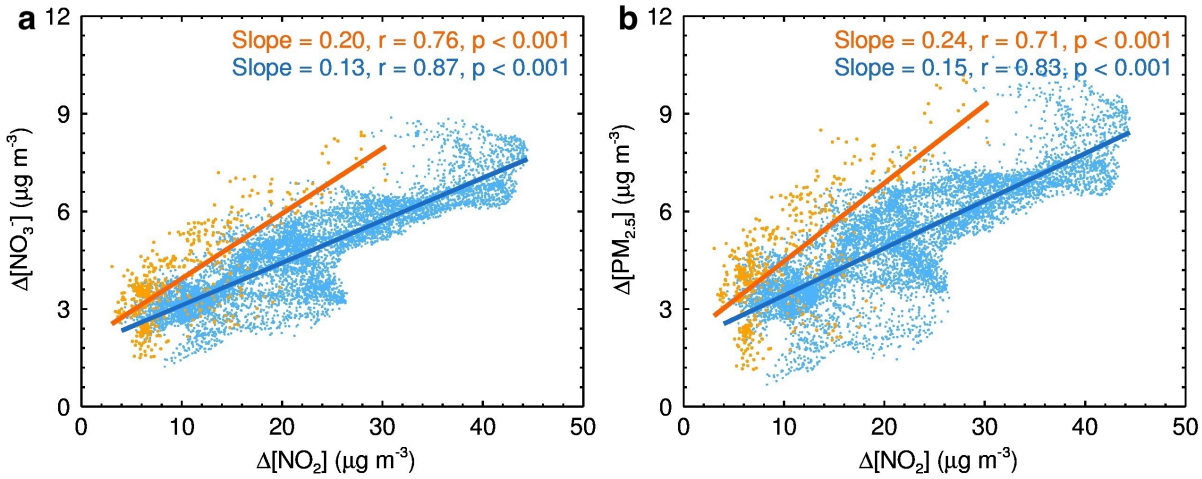

Figure 11. Changes in surface NO_2 and related aerosol-chemistry products during March 2020 over the NCP. (a) Comparison of NO_2 conversion to nitrate aerosol (NO_3^-) formation between agricultural and urban areas, i.e., $\Delta[NO_3^-]/\Delta[NO_2]$ = 0.20 in urban areas and $\Delta[NO_3^-]/\Delta[NO_2]$ = 0.13 in agricultural areas, indicates that change in nitrate in urban areas are more sensitive to the change in NO_2 concentration and NO_2 conversion to NO_3^- is more efficient. (b) NO_2 conversion to $PM_{2.5}$ formation is similar to (a), because nitrate aerosol is the most affected among the various aerosol constituents. The blue and orange colors correspond to the agricultural and urban areas, respectively.

4 Summary and Conclusions

Impact of soil NO_x emissions from agricultural fertilization on the atmospheric environment remains unclear worldwide (Guo et al., 2020; Huang et al., 2018; Sha et al., 2021; Shen et al., 2023). In particular, this issue has not yet received enough attention in China, where substantial N-fertilizers are year by year consumed due to extensive agricultural cultivation areas (Sun et al., 2022; Vitousek et al., 2009; Zhao et al., 2006). Our results indicate that agricultural fertilization is highly responsible for the periodic pulse of the atmospheric NO_2 column in the NCP over the past two decades. A two-decade record of fertilization events at a research station and model results both provide evidence consistent with a cause-to-effect relationship. For example, the fertilization timing is found to match well with the occurrence of satellite-derived NO_2 column pulse in the region. Moreover, the model reasonably captures the regular sub-peak of the NO_2 column in March by introducing an independent module that specifically describes soil NO_x emissions from agricultural fertilization.

These additional NO_x emissions released by croplands directly lead to an elevated level of surface NO_x concentrations. Consequently, the increased atmospheric NO_x concentration significantly inhibits O_3 production in early spring, distinct from the impacts in summer (Sha et al., 2021; Wang et al., 2022), but enhances nitrate formation. For example, soil emissions linked to agricultural fertilization dramatically reduce nighttime O_3 concentrations by 30.1 μg m^{-3} and 15.0 μg m^{-3} in croplands and urban areas, respectively. During daytime, the decreased O_3 concentration is 15.6 μg m^{-3} and 9.7 μg m^{-3}, respectively. In contrast, soil emissions elevate ambient $PM_{2.5}$ concentrations by more than 4.5 μg m^{-3}, accounting for 12% of the $PM_{2.5}$ mass over the NCP in March 2020. The opposite effects are challengeable for China to improve air quality, because China is the world's largest consumer of food, of which food production strongly depends on N-fertilizers input. As the emission from fossil fuel combustion has been gradually decreasing, emissions from agricultural fertilization are with increasing implications for air quality. We thus highlight that reducing NO_x emissions from agricultural fertilization is

of great importance to air quality improvement. In China, the excessive use of N-fertilizer still remains severe (Sun et al., 2022; Vitousek et al., 2009; Zhao et al., 2006), though a lot of efforts have taken to increase the N-fertilizer efficiency and to reduce N losses from fertilizer (Li et al., 2018; Qiao et al., 2022; YAN et al., 2008). Fortunately, the consumption of N-fertilizer reached its peak in 2014 in China and has been decreasing since then (Yu et al., 2022). Policymakers should manage to further reduce emissions from N-fertilizers application, for example, improving N-fertilizers efficiency and developing alternative fertilizers friendly to the environment are highly necessary. These measures will greatly minimize the adverse effects of agricultural fertilization on air quality, human health, and the ecological environment. Nevertheless, one should be aware of the limitation in the present case study that there are only three months of simulation as the basis for all of the insights into the soil NO_x emission and its influences on atmospheric chemistry and composition. More studies in terms of soil NO_x emissions, particularly during springtime, are in need to validate and generalize our model results.

Data availability

The OMI satellite data are from the NASA Goddard Space Flight Center, Goddard Earth Sciences Data and Information Services Center (GES DISC) (https://disc.gsfc.nasa.gov/datasets/OMI_MINDS_NO2d_1.1/summary) and the IASI satellite observations are from the IASI Portal (https://iasi.aeris-data.fr/nh3_iasi_a_arch). The real-time hourly air pollutant measurements including NO_2, O_3, and $PM_{2.5}$ are released by Ministry of Ecology and Environment, China and can be accessed on the website https://quotsoft.net/air/. The MEIC Group and the EDGAR Team for the MEIC and HATP emission inventories which are available at http://www.meicmodel.org and https://edgar.jrc.ec.europa.eu/dataset_htap_v3, respectively.

Author contribution

TF and GL conceptualized the ideas, verified the conclusions, and revised the paper. TF conducted research, designed the experiments, carried out the methodology, performed the simulation, processed the data, prepared the data visualization, and prepared the paper, with contributions from all authors. SZ and NB provided the treatment of meteorological data, analyzed the study data, validated the model performance, and reviewed the paper. XL, YP, YS, and RW provided the observation data and emission inventories, and reviewed the paper. XT and LM provided critical reviews in the pre-publication stage.

Competing interests

The authors declare no conflicts of interest relevant to this study.

Acknowledgments

This work was supported by the National Natural Science Foundation of China (Grants 42371080 and 42371093), the Natural Science Foundation of Shaanxi Province (Grant 2017JM4023), the Natural Science Foundation of Ningbo Municipality (2023J208), and the Science and Technology Innovation 2025 Major Project of Ningbo Municipality (Grants 2022Z032, 2022Z189, and 2023Z139). This study was also sponsored by K. C. Wong Magna Fund in Ningbo University.

References

Almaraz, M., Bai, E., Wang, C., Trousdell, J., Conley, S., Faloona, I. and Houlton, B. Z.: Agriculture is a major source of NOx pollution in California, Sci Adv, 4(1), eaao3477, doi:10.1126/sciadv.aao3477, 2018.

Anderson, I. C. and Levine, J. S.: Simultaneous field measurements of biogenic emissions of

601 nitric oxide and nitrous oxide, J Geophys Res, 92, 965–976, doi:10.1029/JD092iD01p00965,
602 1987.

603 Bauwens, M., Compernolle, S., Stavrakou, T., Müller, J. F., van Gent, J., Eskes, H., Levelt,
604 P. F., van der A, R., Veefkind, J. P., Vlietinck, J., Yu, H. and Zehner, C.: Impact of
605 Coronavirus Outbreak on NO_2 Pollution Assessed Using TROPOMI and OMI Observations,
606 Geophys. Res. Lett., 47(1), e87978, doi:10.1029/2020GL087978, 2020.

607 Bennetzen, E. H., Smith, P. and Porter, J. R.: Decoupling of greenhouse gas emissions from
608 global agricultural production: 1970-2050, Global Change Biol, 22(2), 763–781,
609 doi:10.1111/gcb.13120, 2016.

610 Bouwman, A. F., Boumans, L. J. M. and Batjes, N. H.: Modeling global annual N_2O and NO
611 emissions from fertilized fields, Global Biogeochem. Cycles, 16(4), 1080–28–9,
612 doi:10.1029/2001GB001812, 2002.

613 Buchholz, R. R., Emmons, L. K., Tilmes, S. and The CESM Development Team:
614 CESM2.1/CAM-chem Instantaneous Output for Boundary Conditions, UCARNCAR -
615 Atmospheric Chemistry Observations and Modeling Laboratory, doi:10.5065/NMP7-EP60,
616 2019.

617 Cárdenas, L., Rondón, A., Johansson, C. and Sanhueza, E.: Effects of soil moisture,
618 temperature, and inorganic nitrogen on nitric oxide emissions from acidic tropical savannah
619 soils, J Geophys Res, 98(D8), 14783–14790, doi:10.1029/93JD01020, 1993.

620 Chen, F. and Dudhia, J.: Coupling an advanced land surface-hydrology model with the Penn
621 State-NCAR MM5 modeling system. Part II: Preliminary model validation, Mon. Weather
622 Rev., 129(4), 569–585, doi:10.1175/1520-0493(2001)129<0569:caalsh>2.0.co;2, 2001.

623 Chou, M.-D. and Suarez, M. J.: A solar radiation parameterization for atmospheric studies,
624 edited by M. J. Suarez. 1999.

625 Chou, M.-D., Suarez, M. J., Liang, X.-Z. and Yan, M. M. H.: A thermal infrared radiation
626 parameterization for atmospheric studies, edited by M. J. Suarez. 2001.

627 Clarisse, L., Franco, B., Van Damme, M., Di Gioacchino, T., Hadji-Lazaro, J., Whitburn, S.,
628 Noppen, L., Hurtmans, D., Clerbaux, C. and Coheur, P.: The IASI NH_3 version 4 product:
629 averaging kernels and improved consistency, Atmos. Meas. Tech., 16(21), 5009–5028,
630 doi:10.5194/amt-16-5009-2023, 2023.

631 Crippa, M., Guizzardi, D., Butler, T., Keating, T., Wu, R., Kaminski, J., Kuenen, J.,
632 Kurokawa, J., Chatani, S., Morikawa, T., Pouliot, G., Racine, J., Moran, M. D., Klimont, Z.,
633 Manseau, P. M., Mashayekhi, R., Henderson, B. H., Smith, S. J., Suchyta, H., Muntean, M.,
634 Solazzo, E., Banja, M., Schaaf, E., Pagani, F., Woo, J.-H., Kim, J., Monforti-Ferrario, F.,
635 Pisoni, E., Zhang, J., Niemi, D., Sassi, M., Ansari, T. and Foley, K.: The HTAP_v3 emission

636 mosaic: merging regional and global monthly emissions (2000–2018) to support air quality
637 modelling and policies, Earth System Science Data, 15(6), 2667–2694, doi:10.5194/essd-15-
638 2667-2023, 2023.

639 Davidson, E. A.: Sources of nitric oxide and nitrous oxide following wetting of dry soil, Soil
640 Science Society of America Journal, 56(1), 95–102,
641 doi:10.2136/sssaj1992.03615995005600010015x, 1992.

642 Davidson, E. A., Potter, C. S., Schlesinger, P. and Klooster, S. A.: Model estimates of
643 regional nitric oxide emissions from soils of the southeastern United States, Ecological
644 Applications, 8(3), 748–759, doi:10.1890/1051-0761(1998)008[0748:MEORNO]2.0.CO;2,
645 1998.

646 Emmons, L. K., Schwantes, R. H., Orlando, J. J., Tyndall, G., Kinnison, D., Lamarque, J.-F.,
647 Marsh, D., Mills, M. J., Tilmes, S., Bardeen, C., Buchholz, R. R., Conley, A., Gettelman, A.,
648 Garcia, R., Simpson, I., Blake, D. R., Meinardi, S. and Pétron, G.: The Chemistry Mechanism
649 in the Community Earth System Model Version 2 (CESM2), J. Adv. Model. Earth Syst.,
650 12(4), e2019MS001882, doi:10.1029/2019MS001882, 2020.

651 Feng, T., Bei, N., Zhao, S., Wu, J., Li, X., Zhang, T., Cao, J., Zhou, W. and Li, G.:
652 Wintertime nitrate formation during haze days in the Guanzhong basin, China: A case study,
653 Environ. Pollut., 243, 1057–1067, doi:10.1016/j.envpol.2018.09.069, 2018.

654 Feng, T., Zhao, S., Hu, B., Bei, N., Zhang, X., Wu, J., Li, X., Liu, L., Wang, R., Tie, X. and
655 Li, G.: Assessment of Atmospheric Oxidizing Capacity Over the Beijing-Tianjin-Hebei
656 (BTH) Area, China, J. Geophys. Res. Atmos., 126(7), e2020JD033834,
657 doi:10.1029/2020JD033834, 2021.

658 Feng, T., Zhao, S., Liu, L., Long, X., Gao, C. and Wu, N.: Nitrous acid emission from soil
659 bacteria and related environmental effect over the North China Plain, Chemosphere, 287,
660 132034, doi:10.1016/j.chemosphere.2021.132034, 2022.

661 Fu, X., Wang, T., Gao, J., Wang, P., Liu, Y., Wang, S., Zhao, B. and Xue, L.: Persistent
662 Heavy Winter Nitrate Pollution Driven by Increased Photochemical Oxidants in Northern
663 China, Environ. Sci. Technol., 54(7), 3881–3889, doi:10.1021/acs.est.9b07248, 2020.

664 Galbally, I. E. and Roy, C. R.: Loss of fixed nitrogen from soils by nitric oxide exhalation,
665 Nature, 275(5), 734–735, doi:10.1038/275734a0, 1978.

666 Guenther, A., Karl, T., Harley, P., Wiedinmyer, C., Palmer, P. I. and Geron, C.: Estimates of
667 global terrestrial isoprene emissions using MEGAN (Model of Emissions of Gases and
668 Aerosols from Nature), Atmos. Chem. Phys., 6(11), 3181–3210, doi:10.5194/acp-6-3181-
669 2006, 2006.

670 Guo, L., Chen, J., Luo, D., Liu, S., Lee, H. J., Motallebi, N., Fong, A., Deng, J., Rasool, Q.

671 Z., Avise, J. C., Kuwayama, T., Croes, B. E. and FitzGibbon, M.: Assessment of Nitrogen
672 Oxide Emissions and San Joaquin Valley $PM_{2.5}$ Impacts From Soils in California, J.
673 Geophys. Res. Atmos., 125(24), e2020JD033304, doi:10.1029/2020JD033304, 2020.

674 Hall, S. J., Matson, P. A. and Roth, P. M.: NOx EMISSIONS FROM SOIL: Implications for
675 Air Quality Modeling in Agricultural Regions, Annu. Rev. Energy. Environ., 21(1), 311–346,
676 doi:10.1146/annurev.energy.21.1.311, 1996.

677 Hickman, J. E., Huang, Y., Wu, S., Diru, W., Groffman, P. M., Tully, K. L. and Palm, C. A.:
678 Nonlinear response of nitric oxide fluxes to fertilizer inputs and the impacts of agricultural
679 intensification on tropospheric ozone pollution in Kenya, Global Change Biol, 23(8), 3193–
680 3204, doi:10.1111/gcb.13644, 2017.

681 Hong, S. Y. and Lim, J.: The WRF single-moment 6-class microphysics scheme (WSM6),
682 Asia-Pac. J. Atmos. Sci., 42(2), 129–151, 2006.

683 Huang, L., Fang, J., Liao, J., Yarwood, G., Chen, H., Wang, Y. and Li, L.: Insights into soil
684 NO emissions and the contribution to surface ozone formation in China, Atmos. Chem.
685 Phys., 23(23), 14919–14932, doi:10.5194/acp-23-14919-2023, 2023.

686 Huang, X., Song, Y., Li, M., Li, J., Huo, Q., Cai, X., Zhu, T., Hu, M. and Zhang, H.: A high-
687 resolution ammonia emission inventory in China, Global Biogeochem. Cycles, 26(1),
688 GB1030, doi:10.1029/2011GB004161, 2012.

689 Huang, Y., Hickman, J. E. and Wu, S.: Impacts of enhanced fertilizer applications on
690 tropospheric ozone and crop damage over sub-Saharan Africa, Atmos. Environ., 180, 117–
691 125, doi:10.1016/j.atmosenv.2018.02.040, 2018.

692 Huber, D. E., Steiner, A. L. and Kort, E. A.: Daily Cropland Soil NOx Emissions Identified
693 by TROPOMI and SMAP, Geophys. Res. Lett., 47(2), e89949, doi:10.1029/2020GL089949,
694 2020.

695 Hudman, R. C., Moore, N. E., Mebust, A. K., Martin, R. V., Russell, A. R., Valin, L. C. and
696 Cohen, R. C.: Steps towards a mechanistic model of global soil nitric oxide emissions:
697 implementation and space based-constraints, Atmos. Chem. Phys., 12(1), 7779–7795,
698 doi:10.5194/acp-12-7779-2012, 2012.

699 IPCC: Short-lived Climate Forcers, in Climate Change 2021 – The Physical Science Basis:
700 Working Group I Contribution to the Sixth Assessment Report of the Intergovernmental
701 Panel on Climate Change, pp. 817–922, Cambridge University Press, Cambridge. 2023.

702 Janjić, Z. I.: Nonsingular implementation of the Mellor–Yamada level 2.5 scheme in the
703 NCEP Meso model. 2002.

704 Janssens-Maenhout, G., Crippa, M., Guizzardi, D., Dentener, F., Muntean, M., Pouliot, G.,

Keating, T., Zhang, Q., Kurokawa, J., Wankmüller, R., Denier van der Gon, H., Kuenen, J. J. P., Klimont, Z., Frost, G., Darras, S., Koffi, B. and Li, M.: HTAP-v2.2: A mosaic of regional and global emission grid maps for 2008 and 2010 to study hemispheric transport of air pollution, Atmos. Chem. Phys., 15(19), 11411–11432, doi:10.5194/acp-15-11411-2015, 2015.

Kurokawa, J. and Ohara, T.: Long-term historical trends in air pollutant emissions in Asia: Regional Emission inventory in ASia (REAS) version 3, Atmos. Chem. Phys., 20(21), 12761–12793, doi:10.5194/acp-20-12761-2020, 2020.

Lamsal, L. N., Krotkov, N. A., Vasilkov, A., Marchenko, S., Qin, W., Yang, E.-S., Fasnacht, Z., Joiner, J., Choi, S., Haffner, D., Swartz, W. H., Fisher, B. and Bucsela, E.: Ozone Monitoring Instrument (OMI) Aura nitrogen dioxide standard product version 4.0 with improved surface and cloud treatments, Atmos. Meas. Tech., 14(1), 455–479, doi:10.5194/amt-14-455-2021, 2021.

Laville, P., Lehuger, S., Loubet, B., Chaumartin, F. and Cellier, P.: Effect of management, climate and soil conditions on N2O and NO emissions from an arable crop rotation using high temporal resolution measurements, Agr Forest Meteorol, 151(2), 228–240, doi:10.1016/j.agrformet.2010.10.008, 2011.

Li, G., Bei, N., Cao, J., Wu, J., Long, X., Feng, T., Dai, W., Liu, S., Zhang, Q. and Tie, X.: Widespread and persistent ozone pollution in eastern China during the non-winter season of 2015: observations and source attributions, Atmos. Chem. Phys., 17(4), 2759–2774, doi:10.5194/acp-17-2759-2017, 2017a.

Li, G., Bei, N., Tie, X. and Molina, L. T.: Aerosol effects on the photochemistry in Mexico City during MCMA-2006/MILAGRO campaign, Atmos. Chem. Phys., 11(11), 5169–5182, doi:10.5194/acp-11-5169-2011, 2011a.

Li, G., Lei, W., Bei, N. and Molina, L. T.: Contribution of garbage burning to chloride and $PM_{2.5}$ in Mexico City, Atmos. Chem. Phys., 12(18), 8751–8761, doi:10.5194/acp-12-8751-2012, 2012.

Li, G., Lei, W., Zavala, M., Volkamer, R., Dusanter, S., Stevens, P. and Molina, L. T.: Impacts of HONO sources on the photochemistry in Mexico City during the MCMA-2006/MILAGO Campaign, Atmos. Chem. Phys., 10(14), 6551–6567, doi:10.5194/acp-10-6551-2010, 2010.

Li, G., Zavala, M., Lei, W., Tsimpidi, A. P., Karydis, V. A., Pandis, S. N., Canagaratna, M. R. and Molina, L. T.: Simulations of organic aerosol concentrations in Mexico City using the WRF-CHEM model during the MCMA-2006/MILAGRO campaign, Atmos. Chem. Phys., 11(8), 3789–3809, doi:10.5194/acp-11-3789-2011, 2011b.

Li, M., Liu, H., Geng, G., Hong, C., Liu, F., Song, Y., Tong, D., Zheng, B., Cui, H., Man, H.,

741 Zhang, Q. and He, K.: Anthropogenic emission inventories in China: A review, National
742 Science Review, 4(6), 834–866, doi:10.1093/nsr/nwx150, 2017b.

743 Li, M., Zhang, Q., Kurokawa, J.-I., Woo, J.-H., He, K., Lu, Z., Ohara, T., Song, Y., Streets,
744 D. G., Carmichael, G. R., Cheng, Y., Hong, C., Huo, H., Jiang, X., Kang, S., Liu, F., Su, H.
745 and Zheng, B.: MIX: a mosaic Asian anthropogenic emission inventory under the
746 international collaboration framework of the MICS-Asia and HTAP, Atmos. Chem. Phys.,
747 17(2), 935–963, doi:10.5194/acp-17-935-2017, 2017c.

748 Li, T., Zhang, W., Yin, J., Chadwick, D., Norse, D., Lu, Y., Liu, X., Chen, X., Zhang, F.,
749 Powlson, D. and Dou, Z.: Enhanced-efficiency fertilizers are not a panacea for resolving the
750 nitrogen problem, Global Change Biol, 24(2), e511–e521, doi:10.1111/gcb.13918, 2018.

751 Liu, C., Zheng, X., Zhou, Z., Han, S., Wang, Y., Wang, K., Liang, W., Li, M., Chen, D. and
752 Yang, Z.: Nitrous oxide and nitric oxide emissions from an irrigated cotton field in Northern
753 China, Plant Soil, 332(1), 123–134, doi:10.1007/s11104-009-0278-5, 2010.

754 Liu, L., Wu, J., Liu, S., Li, X., Zhou, J., Feng, T., Qian, Y., Cao, J., Tie, X. and Li, G.:
755 Effects of organic coating on the nitrate formation by suppressing the N_2O_5 heterogeneous
756 hydrolysis: a case study during wintertime in Beijing–Tianjin–Hebei (BTH), Atmos. Chem.
757 Phys., 19(12), 8189–8207, doi:10.5194/acp-19-8189-2019, 2019.

758 Liu, X. J., Mosier, A. R., Halvorson, A. D. and Zhang, F. S.: Tillage and Nitrogen
759 Application Effects on Nitrous and Nitric Oxide Emissions from Irrigated Corn Fields, Plant
760 Soil, 276(1), 235–249, doi:10.1007/s11104-005-4894-4, 2005.

761 Liu, X., Ju, X., Zhang, F., Pan, J. and Christie, P.: Nitrogen dynamics and budgets in a winter
762 wheat–maize cropping system in the North China Plain, Field Crops Research, 83(2), 111–
763 124, doi:10.1016/S0378-4290(03)00068-6, 2003.

764 Liu, X., Zhang, Y., Han, W., Tang, A., Shen, J., Cui, Z., Vitousek, P., Erisman, J. W.,
765 Goulding, K., Christie, P., Fangmeier, A. and Zhang, F.: Enhanced nitrogen deposition over
766 China, Nature, 494(7438), 459–462, doi:10.1038/nature11917, 2013.

767 Lu, X., Ye, X., Zhou, M., Zhao, Y., Weng, H., Kong, H., Li, K., Gao, M., Zheng, B., Lin, J.,
768 Zhou, F., Zhang, Q., Wu, D., Zhang, L. and Zhang, Y.: The underappreciated role of
769 agricultural soil nitrogen oxide emissions in ozone pollution regulation in North China, Nat.
770 Commun., 12(1), 5021–9, doi:10.1038/s41467-021-25147-9, 2021.

771 Ma, R., Yu, K., Xiao, S., Liu, S., Ciais, P. and Zou, J.: Data-driven estimates of fertilizer-
772 induced soil NH_3 , NO and N_2O emissions from croplands in China and their climate change
773 impacts, Global Change Biol, 28(3), 1008–1022, doi:10.1111/gcb.15975, 2022.

774 Matson, P. A., Naylor, R. and Ortiz-Monasterio, I.: Integration of Environmental,
775 Agronomic, and Economic Aspects of Fertilizer Management, Science, 280(5360), 112–115,

776 doi:10.1126/science.280.5360.112, 1998.

777 Murray, L. T., Jacob, D. J., Logan, J. A., Hudman, R. C. and Koshak, W. J.: Optimized
778 regional and interannual variability of lightning in a global chemical transport model
779 constrained by LIS/OTD satellite data, J. Geophys. Res. Atmos., 117(D), D20307,
780 doi:10.1029/2012JD017934, 2012.

781 Oikawa, P. Y., Ge, C., Wang, J., Eberwein, J. R., Liang, L. L., Allsman, L. A., Grantz, D. A.
782 and Jenerette, G. D.: Unusually high soil nitrogen oxide emissions influence air quality in a
783 high-temperature agricultural region, Nat. Commun., 6(1), 8753–10,
784 doi:10.1038/ncomms9753, 2015.

785 Potter, P., Ramankutty, N., Bennett, E. M. and Donner, S. D.: Characterizing the Spatial
786 Patterns of Global Fertilizer Application and Manure Production, Earth Interactions, 14, 1–
787 22, doi:10.1175/2009EI288.1, 2010.

788 Qiao, J., Wang, J., Zhao, D., Zhou, W., Schwenke, G., Yan, T. and De Li Liu: Optimizing N
789 fertilizer rates sustained rice yields, improved N use efficiency, and decreased N losses via
790 runoff from rice-wheat cropping systems, Agriculture, Ecosystems & Environment, 324,
791 107724, doi:10.1016/j.agee.2021.107724, 2022.

792 Seinfeld, J. H. and Pandis, S. N.: Atmospheric Chemistry and Physics - From Air Pollution to
793 Climate Change, 2nd ed., John Wiley & Sons, New Jersey. 2006.

794 Sha, T., Ma, X., Zhang, H., Janechek, N., Wang, Y., Wang, Y., Castro García, L., Jenerette,
795 G. D. and Wang, J.: Impacts of Soil NOx Emission on O_3 Air Quality in Rural California,
796 Environ. Sci. Technol., 55(10), 7113–7122, doi:10.1021/acs.est.0c06834, 2021.

797 Shen, Y., Xiao, Z., Wang, Y., Xiao, W., Yao, L. and Zhou, C.: Impacts of Agricultural Soil
798 NOx Emissions on O3 Over Mainland China, J. Geophys. Res. Atmos., 128(4),
799 e2022JD037986, doi:https://doi.org/10.1029/2022JD037986, 2023.

800 Sillman, S.: The use of NOy , H2O2, and HNO3 as indicators for ozone-NOx-hydrocarbon
801 sensitivity in urban locations, J. Geophys. Res. Atmos., 100(D7), 14175–14188,
802 doi:10.1029/94JD02953, 1995.

803 Steinkamp, J. and Lawrence, M. G.: Improvement and evaluation of simulated global
804 biogenic soil NO emissions in an AC-GCM, Atmos. Chem. Phys., 11(1), 6063–6082,
805 doi:10.5194/acp-11-6063-2011, 2011.

806 Sun, X., Ritzema, H., Huang, X., Bai, X. and Hellegers, P.: Assessment of farmers' water and
807 fertilizer practices and perceptions in the North China Plain, Irrigation and Drainage, 71(4),
808 980–996, doi:https://doi.org/10.1002/ird.2719, 2022.

809 Tan, W., Wang, H., Su, J., Sun, R., He, C., Lu, X., Lin, J., Xue, C., Wang, H., Liu, Y., Liu,

L., Zhang, L., Wu, D., Mu, Y. and Fan, S.: Soil Emissions of Reactive Nitrogen Accelerate Summertime Surface Ozone Increases in the North China Plain, Environ. Sci. Technol., 57(34), 12782–12793, doi:10.1021/acs.est.3c01823, 2023.

Tang, K., Qin, M., Fang, W., Duan, J., Meng, F., Ye, K., Zhang, H., Xie, P., Liu, J., Liu, W., Feng, Y., Huang, Y. and Ni, T.: An automated dynamic chamber system for exchange flux measurement of reactive nitrogen oxides (HONO and NOx) in farmland ecosystems of the Huaihe River Basin, China, Sci. Total Environ., 745(C), 140867, doi:10.1016/j.scitotenv.2020.140867, 2020.

Tian, D., Zhang, Y., Mu, Y., Liu, J. and He, K.: Effect of N fertilizer types on N_2O and NO emissions under drip fertigation from an agricultural field in the North China Plain, Sci. Total Environ., 715(C), 136903, doi:10.1016/j.scitotenv.2020.136903, 2020.

Tubiello, F. N., Salvatore, M., Rossi, S., Ferrara, A., Fitton, N. and Smith, P.: The FAOSTAT database of greenhouse gas emissions from agriculture, Environ. Res. Lett., 8(1), 015009, doi:10.1088/1748-9326/8/1/015009, 2013.

Vinken, G. C. M., Boersma, K. F., Maasakkers, J. D., Adon, M. and Martin, R. V.: Worldwide biogenic soil NOx emissions inferred from OMI NO_2 observations, Atmos. Chem. Phys., 14(1), 10363–10381, doi:10.5194/acp-14-10363-2014, 2014.

Vitousek, P. M., Naylor, R., Crews, T., David, M. B., Drinkwater, L. E., Holland, E., Johnes, P. J., Katzenberger, J., Martinelli, L. A., Matson, P. A., Nziguheba, G., Ojima, D., Palm, C. A., Robertson, G. P., Sanchez, P. A., Townsend, A. R. and Zhang, F. S.: Nutrient Imbalances in Agricultural Development, Science, 324, 1519–1520, doi:10.1126/science.1170261, 2009.

Wang, R., Bei, N., Wu, J., Li, X., Liu, S., Yu, J., Jiang, Q., Tie, X. and Li, G.: Cropland nitrogen dioxide emissions and effects on the ozone pollution in the North China plain, Environ. Pollut., 294, 118617, doi:10.1016/j.envpol.2021.118617, 2022.

Wen, L., Xue, L., Wang, X., Xu, C., Chen, T., Yang, L., Wang, T., Zhang, Q. and Wang, W.: Summertime fine particulate nitrate pollution in the North China Plain: increasing trends, formation mechanisms and implications for control policy, Atmos. Chem. Phys., 18(15), 11261–11275, doi:10.5194/acp-18-11261-2018, 2018.

Wu, J., Bei, N., Hu, B., Liu, S., Wang, Y., Shen, Z., Li, X., Liu, L., Wang, R., Liu, Z., Cao, J., Tie, X., Molina, L. T. and Li, G.: Aerosol–photolysis interaction reduces particulate matter during wintertime haze events, Proc. Natl. Acad. Sci. U.S.A., 117(18), 9755–9761, doi:10.1073/pnas.1916775117, 2020.

YAN, X., JIN, J.-Y., He, P. and LIANG, M.-Z.: Recent Advances on the Technologies to Increase Fertilizer Use Efficiency, Agricultural Sciences in China, 7(4), 469–479, doi:10.1016/S1671-2927(08)60091-7, 2008.

Yan, X., Ohara, T. and Akimoto, H.: Statistical modeling of global soil NOx emissions, Global Biogeochem. Cycles, 19(3), GB3019, doi:10.1029/2004GB002276, 2005.

Yienger, J. J. and Levy, H.: Empirical model of global soil-biogenic NOx emissions, J. Geophys. Res. Atmos., 100(D), 11447–11464, doi:10.1029/95JD00370, 1995.

Yu, Z., Liu, J. and Kattel, G.: Historical nitrogen fertilizer use in China from 1952 to 2018, Earth System Science Data, 14(11), 5179–5194, doi:10.5194/essd-14-5179-2022, 2022.

Zhang, Q., Streets, D. G. and Carmichael, G. R.: Asian emissions in 2006 for the NASA INTEX-B mission, Atmos. Chem. Phys., 9(14), 5131–5153, doi:10.5194/acp-9-5131-2009, 2009.

Zhang, R., Wang, G., Guo, S., Zamora, M. L., Ying, Q., Lin, Y., Wang, W., Hu, M. and Wang, Y.: Formation of urban fine particulate matter, Chem. Rev., 115(10), 3803–3855, doi:10.1021/acs.chemrev.5b00067, 2015.

Zhang, Y., Liu, J., Mu, Y., Pei, S., Lun, X. and Chai, F.: Emissions of nitrous oxide, nitrogen oxides and ammonia from a maize field in the North China Plain, Atmos. Environ., 45(17), 2956–2961, doi:10.1016/j.atmosenv.2010.10.052, 2011.

Zhao, M., Tian, Y., Zhang, M., Yao, Y., Ao, Y., Bin Yin and Zhu, Z.: Nonlinear response of nitric oxide emissions to a nitrogen application gradient: A case study during the wheat season in a Chinese rice-wheat rotation system, Atmos. Environ., 102(C), 200–208, doi:10.1016/j.atmosenv.2014.11.052, 2015.

Zhao, R.-F., Chen, X.-P., Zhang, F.-S., Zhang, H., Schroder, J. and Römheld, V.: Fertilization and Nitrogen Balance in a Wheat–Maize Rotation System in North China, Agron. J., 98(4), 938–945, doi:10.2134/agronj2005.0157, 2006.

Zhu, Z., Stewart, B. A. and Fu, X.: Double cropping wheat and corn in a sub-humid region of China, Field Crops Research, 36(3), 175–183, doi:10.1016/0378-4290(94)90109-0, 1994.